

Dynamical vertex approximation

— an introduction —

K. HELD¹, A. A. KATANIN^{2,3}, and A. TOSCHI²

¹ *Institute of Solid State Physics, Vienna University of Technology, 1040 Vienna, Austria*

² *Max-Planck-Institut für Festkörperforschung, 70569 Stuttgart, Germany*

³ *Institute of Metal Physics, 620219 Ekaterinburg, Russia*

(Received Mmmmm DD, YYYY)

We give an elementary introduction to a recent diagrammatic extension of dynamical mean field theory (DMFT) coined dynamical vertex approximation (DFA). This approach contains the important local correlations of DMFT, giving, among others, rise to quasiparticle renormalizations, Mott-Hubbard transitions and magnetism, but also non-local correlations beyond. The latter are at the very essence of many physical phenomena in strongly correlated electron systems. As correlations are treated equally on all length scales, DFA allows us to describe physical phenomena such as magnons, quantum criticality, and the interplay between antiferromagnetism and superconductivity. We review results hitherto obtained for the Hubbard model in dimensions $d = 3, 2$, and 1 .

§1. Introduction

Dynamical mean field theory (DMFT)^{1)–4)} has been a success story for the theoretical modeling of strongly correlated electrons systems since it contains the major contribution of electronic correlations: the local ones. Diagrammatically, DMFT corresponds to all topologically distinct Feynman diagrams, albeit only for their local part. Hence, it is a non-perturbative approach which, from another point of view, can be envisaged as a mean-field theory where the local Coulomb interaction U on all sites but one is replaced by a dynamical (frequency-dependent) mean field given in terms of the self energy Σ . First, DMFT was applied to model Hamiltonians for studying, among others, the Mott-Hubbard transition,^{2),3),5)} magnetism,^{6)–10)} and the strong quasiparticle renormalization of correlated electrons, including the only recently observed kink in the quasiparticle's dispersion relation.^{11)–13)} In the last years, the focus shifted towards the realistic calculation of material properties^{14)–18)} and the inclusion of non-local correlations, which are the topic of our paper.

While usually smaller in absolute terms than the local correlations, the non-local correlations nonetheless become essential at low temperatures where they lead to pertinent correlation effects such as spin fluctuations, magnons, quantum criticality, and (possibly) superconductivity. Actually, many of the most fascinating phenomena of strongly correlated electron systems are driven by non-local correlations.

Two different paths have been followed to extend DMFT by non-local correlations, see Fig. 1. Cluster extensions consider instead of the single DMFT site (the local problem or Anderson impurity model) a couple of sites and take correlations between these sites into account, see Ref. 19) for a review. There are two main vari-

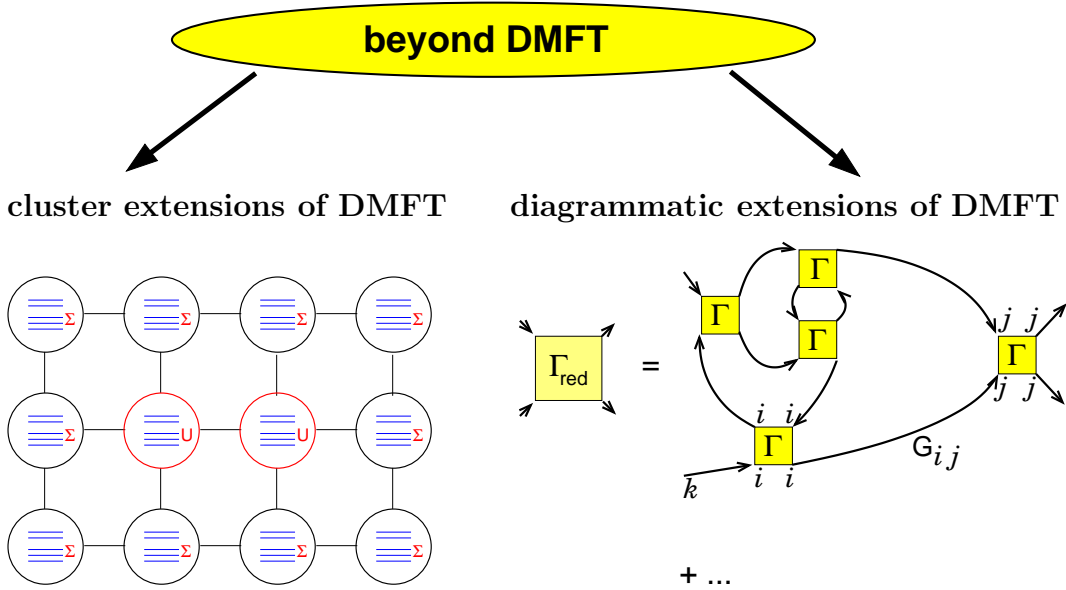


Fig. 1. Two ways to include non-local correlations beyond DMFT. In cluster extensions of DMFT (left), a couple of sites (here two) are embedded in a dynamical mean field which can be formulated through the self energy Σ . Restricted to a single site, DMFT is recovered. In diagrammatic extensions, the local contribution of DMFT is supplemented by certain non-local contributions. Shown is the dynamical vertex approximation (D Γ A) where the fully irreducible vertex is purely local. These local building blocks are connected by non-local Green function lines G_{ij} , resulting in a non-local reducible vertex and self energy. Reducing G_{ij} to its local contribution G_{ii} reproduces DMFT.

ants: cellular (or cluster) DMFT^{20)–22)} where the self energy is directly related to a supercell in real space, and the dynamical cluster approximation (DCA)^{21), 23)–25)} where it is patched in \mathbf{k} space. A generalization in form of a self energy functional approach has been formulated more recently by Potthoff.^{27), 28)} Also the $1/d$ expansion of DMFT^{29), 30)} can be subsumed here since it connects a single-site cluster and a two-site cluster. These approaches have been applied successfully for studying the one-dimensional^{31), 32)} and two-dimensional^{19), 21), 33)–35)} Hubbard model, as well as for the investigation of spin-Peierls physics in Ti_2O_3 ,³⁶⁾ NaV_2O_5 ,³⁷⁾ and VO_2 .³⁸⁾ The biggest drawback of the cluster extensions is their restriction to short-range correlations because the numerical effort is exponentially growing with the number of cluster sites, similar to the direct quantum Monte Carlo simulation³⁹⁾ of the lattice problem. For the one-band Hubbard model, approximately 30-60 sites are possible which means a correlation length of about 3 sites in two dimensions and 1 site in three dimensions. In realistic multi-orbital calculations, the effort increases further with the number of orbitals. Hence, hitherto only two sites have been considered.

Obviously, we need another route to tackle *long-range* correlations. This is possible through diagrammatic extensions of DMFT which were addressed recently by several groups. Kuchinskii *et al.*^{40), 41)} combined the local DMFT self energy of the Hubbard model with the non-local self energy of the spin-Fermion model and in-

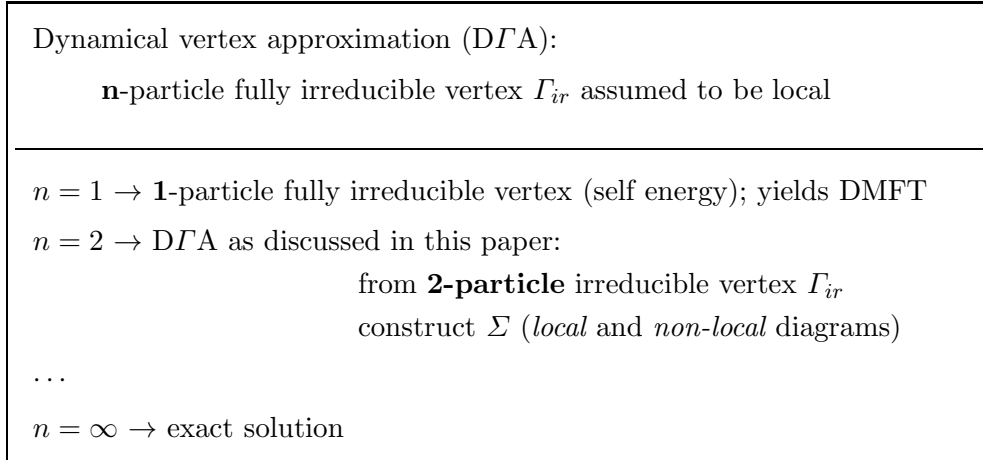
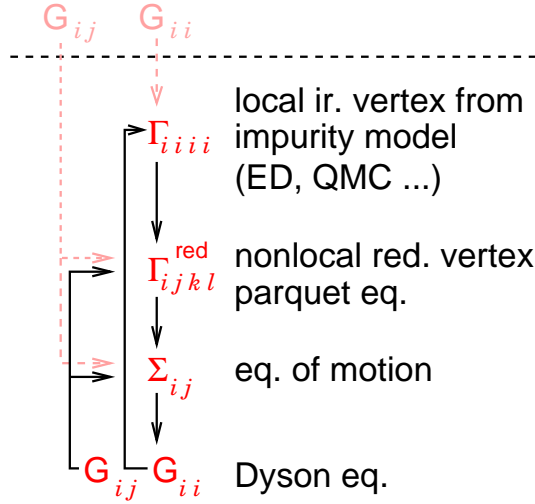


Fig. 2. D Γ A as the natural extension of DMFT to the n -particle fully irreducible vertex.

cluded long-range correlations this way. Rubtsov *et al.*⁴²⁾ proposed a dual Fermion approach to this end. Tokar and Monnier⁴³⁾ developed a perturbative extension which however only includes short-range correlations. We think that a natural extension of DMFT coined dynamical vertex approximation (D Γ A),⁴⁴⁾ which also includes the spin-Fermion diagrams in a systematic way,⁴⁵⁾ is particularly promising. Instead of assuming the one-particle fully irreducible vertex, i.e., the self energy, to be purely local as in DMFT, D Γ A assumes the same for the n -particle fully irreducible vertex Γ_{ir} ,⁴⁴⁾ see Fig. 2. These local building blocks are then connected by non-local Green functions, yielding a non-local reducible vertex and self-energy; see diagrams in the right panel of Fig. 1. Most natural (and feasible) is the case $n = 2$, i.e., the two-particle vertex. But, in principle, implementations with higher n are possible and the exact solution is recovered in the limit $n \rightarrow \infty$. The D Γ A has been proposed by Toschi *et al.*⁴⁴⁾ and independently (with minor differences) by Slezak *et al.*,⁴⁶⁾ who employ a DCA cluster as a starting point and a perturbative calculation of the one-frequency vertex. Very similar ideas including less diagrams have also been put forward independently by Kusunose.⁴⁷⁾

The paper is organized as follows: Section 2 focuses on the D Γ A approach and algorithm, introducing the full version of the approach in Section 2.1, a restriction to the most important diagrams for magnetic fluctuations in Section 2.2, and a Moriya-esque λ correction in Section 2.3. Physical results for the Hubbard model in $d = 3, 2$, and 1 are presented in Sections 3.1, 3.2, and 3.3, respectively. Finally, Section 4 gives a summary and outlook.

Fig. 3. Full (self-consistent) $D\Gamma A$ algorithm.

§2. $D\Gamma A$ algorithm

2.1. Full (self-consistent) $D\Gamma A$

Taking the locality of the fully irreducible^{*)} vertex as a starting point, we can formulate the $D\Gamma A$ approach as following, see Fig. 3 for the algorithm: Starting with an arbitrary local Green function, we first have to calculate the fully irreducible vertex. This is well defined diagrammatically, but in practice one will solve the Anderson impurity model numerically using, for example, the exact diagonalization (ED)⁴⁴⁾ or quantum Monte Carlo simulation (QMC) in its Hirsch-Fye,⁴⁸⁾ projective,⁴⁹⁾ continuous time^{50),51)} or hybrid⁵²⁾ variant. In these numerical approaches, one actually does not compute the irreducible vertex directly, but instead the local three-frequency (generalized) spin and charge susceptibility and from this –through the local parquet equations^{53)–55)}– the fully irreducible vertex; see Ref. 44) for details.

In a second step, the (non-local) reducible vertex is calculated from this (local) fully irreducible vertex. Fig. 1 shows as an example one reducible diagram constructed from the irreducible vertex. But of course, we have to sum over all reducible Feynman diagrams ^{**)} . This can be achieved more elegantly through the parquet equations,^{53)–55)} which is still a challenge for an actual implementation of this full $D\Gamma A$ approach.

Having the non-local reducible vertex, one can easily obtain the non-local $D\Gamma A$ self energy (third step in Fig. 3) through an exact equation which follows from the

^{*)} That is, cutting two Green function lines of the Feynman diagram for the vertex does not divide the vertex into two parts.

^{**)} That is, all Feynman diagrams, which have the local irreducible vertex and the non-local Green function as building blocks, and which do not separate into two parts when cutting two Green function lines.

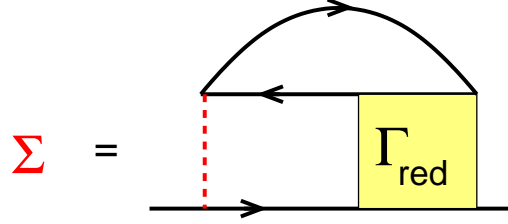


Fig. 4. Diagrammatic representation of the equation of motion connecting reducible vertex and self-energy.

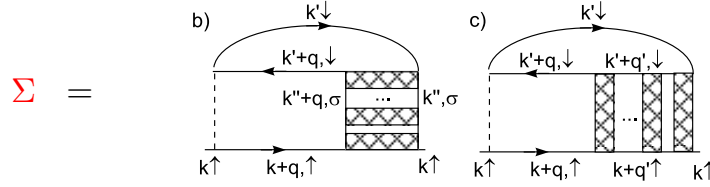


Fig. 5. The two particle-hole channels contributing to the self-energy in the ladder approximation, in the longitudinal and transversal spin channel, respectively. Instead of the bare interaction, ladder diagrams are constructed from the local vertices (crosshatched) irreducible in the corresponding spin and charge channels. [reproduced from Ref. 44)]

Heisenberg equation of motion:^{54),55)}

$$\Sigma_{\mathbf{k},\nu} = U \frac{n}{2} - T^2 U \sum_{\substack{\nu'\omega \\ \mathbf{k}'\mathbf{q}}} \Gamma_{\mathbf{k}\mathbf{k}'\mathbf{q}}^{\nu\nu'\omega\uparrow\downarrow} G_{\mathbf{k}'+\mathbf{q},\nu'+\omega} G_{\mathbf{k}',\nu'} G_{\mathbf{k}+\mathbf{q},\nu+\omega}; \quad (2.1)$$

see Fig. 4 for the diagrammatic representation. Here, \mathbf{k} , \mathbf{k}' , and \mathbf{q} denote the three involved wave vectors; ν , ν' , and ω the corresponding Matsubara frequency; n the number of electrons per site, U the interaction and T the temperature; $\Gamma_{\mathbf{k}\mathbf{k}'\mathbf{q}}^{\nu\nu'\omega}$ is the afore calculated reducible four-point vertex and $G_{\mathbf{k},\nu}$ the Fourier-transform of the non-local Green function G_{ij} taken as a starting point in the first line of Figures 3.

From the self energy Eq. (2.1), the dispersion relation $\epsilon_{\mathbf{k}}$ of the lattice and the chemical potential μ , we can now calculate a new local and non-local Green function via the Dyson equation

$$G_{\mathbf{k},\nu} = [i\nu_n - \epsilon_{\mathbf{k}} + \mu - \Sigma_{\mathbf{k},\nu}]^{-1}. \quad (2.2)$$

After this fourth step of the algorithm, we can go back to step 1 and iterate the DΓA algorithm Fig. 3 until convergence is reached.

2.2. Restriction to the two-particle-hole channels

Instead of this full (self-consistent) DΓA approach, we have, in a first step, implemented a simplified scheme:⁴⁴⁾ Neglecting the particle-particle channel of the Parquet diagrams, we restricted ourselves to the two particle-hole channels which are longitudinal and transversal, respectively, in the spin indices; see Fig. 5 b) and c). This restriction is reasonable for spin fluctuations where these channels are

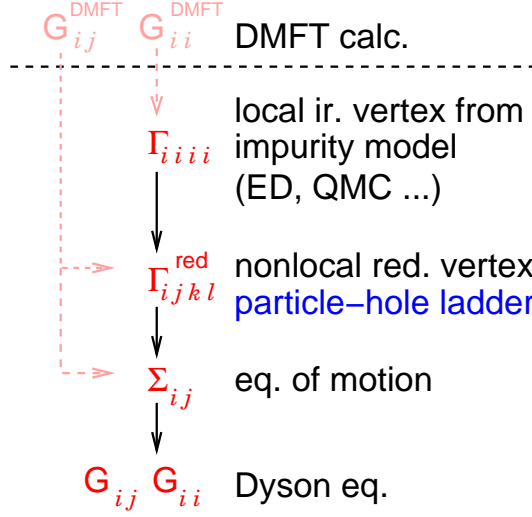


Fig. 6. Restriction of the DΓA algorithm to particle-hole ladder diagrams.

dominating and actually diverging close to the antiferromagnetic phase transition in two dimensions. For other physical phenomena such as superconductivity the particle-particle channel is, as a matter of course, essential.

The algorithm is shown in Fig. 6: We first calculate the irreducible vertex $\Gamma_{s(c),\text{ir}}$ in the spin and charge channel from the numerically obtained susceptibility of the Anderson impurity model (step one in Fig. 6), see Eqs. (9)-(11) of Ref. 44). From this we calculate the reducible vertex $\Gamma_{s(c),\text{q}}^{\nu\nu'\omega}$ (step two in Fig. 6) through the ladder summation which yields

$$\Gamma_{s(c),\text{q}}^{\nu\nu'\omega} = [(\Gamma_{s(c),\text{ir}}^{\nu\nu'\omega})^{-1} - \chi_{0\text{q}\omega}^{\nu'} \delta_{\nu\nu'}]^{-1} \quad (2.3)$$

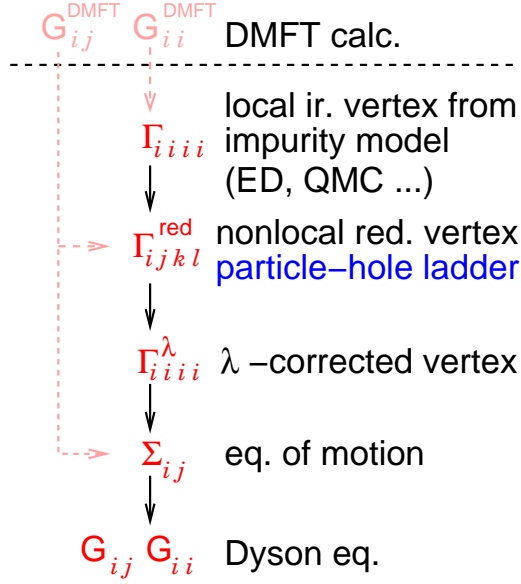
where $\chi_{0\text{q}\omega}^{\nu'} = -T \sum_{\mathbf{k}} G_{\mathbf{k},\nu'} G_{\mathbf{k}+\mathbf{q},\nu'+\omega}$ is the bubble contribution to the susceptibility. In the third step of Fig. 6, the self energy is obtained from these vertices through Eq. (2.1) which yields

$$\begin{aligned} \Sigma_{\mathbf{k},\nu} = & \frac{1}{2}Un + \frac{1}{2}TU \sum_{\nu'\omega,\mathbf{q}} \chi_{0\text{q}\omega}^{\nu'} \left(3\Gamma_{s,\mathbf{q}}^{\nu\nu'\omega} - \Gamma_{c,\mathbf{q}}^{\nu\nu'\omega} \right. \\ & \left. + \Gamma_{c,\text{loc}}^{\nu\nu'\omega} - \Gamma_{s,\text{loc}}^{\nu\nu'\omega} \right) G_{\mathbf{k}+\mathbf{q},\nu+\omega}. \end{aligned} \quad (2.4)$$

for the restriction to the ladder diagrams in the two particle-hole channels of Fig. 5 b) and c), respectively. Here, $\Gamma_{s(c),\text{loc}}$ is the local (\mathbf{q} -summed) counterpart of $\Gamma_{s(c),\text{q}}$. With the restriction to the two particle-hole channels, actually a non-self consistent calculation is preferable so that the algorithm ends with a calculation of the DΓA Green function from the self energy of Eq. (2.4), using the Dyson Eq. (2.2).

2.3. Moriyaeque λ correction

As a numerically inexpensive alternative to the fully self-consistent DΓA algorithm, we recently introduced a Moriyaeque λ correction⁴⁵⁾ to the algorithm of

Fig. 7. DΓA algorithm with Moriya-like λ correction.

Section 2.2. In the Moriya theory of weak itinerant magnets,⁵⁶⁾ the perturbatively obtained susceptibility is corrected as follows

$$\chi_{\mathbf{q}\omega}^s \longrightarrow [(\chi_{\mathbf{q}\omega}^s)^{-1} + \lambda]^{-1}, \quad (2.5)$$

where $\chi_{\mathbf{q}\omega}^s = \sum_{\nu\nu'} \chi_{s\mathbf{q}}^{\nu\nu'}$ is the susceptibility. We do the same but for strongly correlated electron systems in the λ -corrected DΓA. In our approach, the value of λ is fixed by the sumrule

$$- \int_{-\infty}^{\infty} \frac{d\nu}{\pi} \text{Im} \Sigma_{\mathbf{k},\nu} = U^2 n(1 - n/2)/2. \quad (2.6)$$

Eq. (2.5) translates to a λ correction of the vertex via

$$\chi_{s(c),\mathbf{q}}^{\nu\nu'\omega} = [(\chi_{0\mathbf{q}\omega}^{\nu\nu'})^{-1} \delta_{\nu\nu'} - \Gamma_{s(c),\text{ir}}^{\nu\nu'\omega}]^{-1} \quad (2.7)$$

see Ref. 46) for details. Hence in the DΓA algorithm, the λ correction is one additional step, the third step of Fig. 7. Otherwise the algorithm remains unchanged.

Through the λ correction, we include important effects of the self-consistent full DΓA. In particular, the reduction of the magnetic transition temperature. In two dimensions, even the Mermin-Wagner theorem is fulfilled.⁴⁵⁾

§3. Results for the Hubbard model

3.1. Three-dimensional Hubbard model

Let us turn to the results, starting with the three-dimensional Hubbard model on a cubic lattice

$$H = -t \sum_{\langle ij \rangle \sigma} c_{i\sigma}^\dagger c_{j\sigma} + U \sum_i n_{i\uparrow} n_{i\downarrow}. \quad (3.1)$$

Here, t denotes the hopping amplitude between nearest-neighbors, U the Coulomb interaction, $c_{i\sigma}^\dagger (c_{i\sigma})$ creates (annihilates) an electron with spin σ on site i , $n_{i\sigma} = c_{i\sigma}^\dagger c_{i\sigma}$. In the following, we restrict ourselves to the paramagnetic phase with $n = 1$ electron per site at a finite temperature T . One of the cornerstones of strongly correlated electron systems for this paramagnetic phase is the Mott-Hubbard transition,^{57),58)} which was analyzed in DMFT in great detail^{2),3),5)} with some -by now settled- controversy for the multi-orbital case.⁵⁹⁾⁻⁷⁶⁾ What is less clear however is how far antiferromagnetic fluctuations above the ordering temperature affect the Mott-Hubbard transition. For an orientation, see the phase diagram of the Hubbard model in the left inset of Fig. 8. In DMFT, there is no feedback whatsoever of the nearby antiferromagnetic phase onto the spectrum and the self energy in the paramagnetic phase. If we, for example, completely suppress the antiferromagnetic phase through “frustrating” the lattice with longer-range hopping, the DMFT spectrum is the very same^{*)}. DΓA heals this shortcoming of DMFT.

In our calculations,⁴⁴⁾ we considered three points in the paramagnetic phase of the phase diagram, marked as symbols in left inset of Fig. 8. These points are on the metallic side of the Mott-Hubbard transition and in the crossover regime where the metal continuously transforms into an insulator. In DMFT, the metallic side corresponds to a well defined quasiparticle peak (first point considered at $U = 1D$, $\beta \equiv 1/T = 0.067D$, where $D \equiv 2\sqrt{6}t$ is the effective bandwidth/standard deviation of the density of states). When increasing U to the crossover regime, this quasiparticle peak is first strongly damped, i.e, smeared out (second point considered at $U = 1.5D$, $\beta = 0.089D$; for the DMFT spectrum see Fig. 9). Note, this change from a metal to a strongly damped quasi-metal was confirmed recently by photoemission experiments for V_2O_3 by Baldassarre *et al.*⁷⁸⁾ Upon a further increase of U the spectrum develops a pseudogap (third point considered at $U = 2D$, $\beta = 0.1D$). Or, if we take vice versa the insulating gap as a starting point, this insulating gap is filled, see Ref. 77) for an experimental validation by hands of V_2O_3 . Increasing U further, eventually a truly insulating gap is obtained.

In its main panel, Fig. 8 shows the four-point vertex irreducible in the spin channel, which was calculated numerically using exact diagonalization as an impurity solver for the Anderson impurity model.⁴⁴⁾ As we see, the vertex strongly depends on all three frequencies (main panel and right inset). It becomes unexpectedly strong if an increasing U enhances the electronic correlations. Strong local correlations result in a large vertex which, in the vicinity of an antiferromagnetic phase transition,

^{*)} except for changes possibly induced by a change of the density of states due the additional hopping

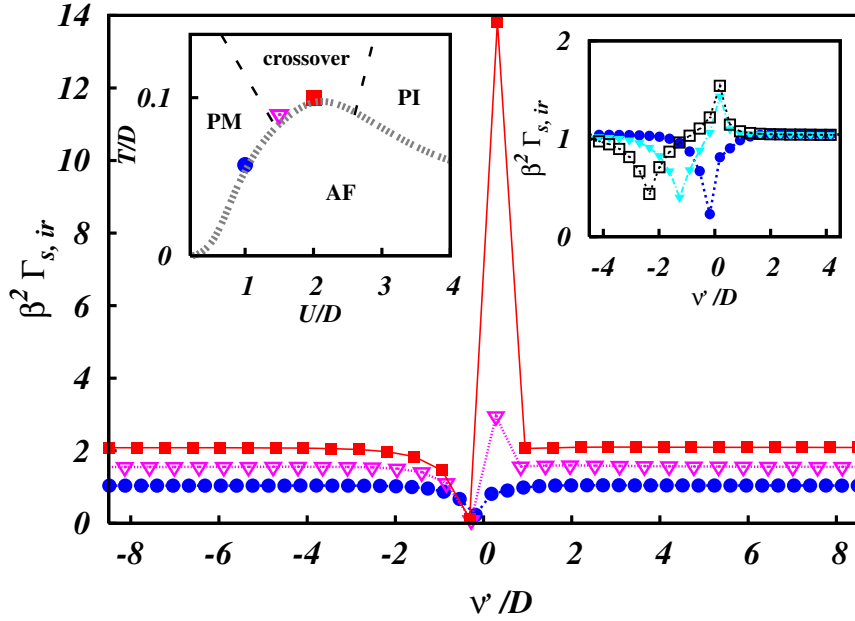


Fig. 8. Dependence of the local irreducible vertex $\Gamma_{s,ir}^{\nu', \nu=\pi/\beta, \omega=0}$ on the incoming Fermionic frequency ν' , for the three different values of U and T indicated as symbols in the left inset, which shows the DMFT phase diagram with paramagnetic metallic (PM), insulating (PI), and antiferromagnetic (AF) phase as well as the crossover region between PM and PI. Right inset: Same as main panel but at fixed $U = 1D$ and at different ω 's (squares: $\omega = 12\pi T$; triangles: $\omega = 6\pi T$; circles $\omega = 0$). [reproduced from Ref. 44)]

entail strong non-local correlations.

As discussed in Section 2.2, we can calculate the D Γ A self energy and k -resolved spectral function from the vertex of Fig. 8. The results for a wave vector $\mathbf{k} = (\pi/2, \pi/2, \pi/2)$ on the Fermi surface are presented in Fig. 9. On the metallic side at $U = 1D$, the non-local antiferromagnetic fluctuations lead to a relatively weak damping of the quasiparticle peak (QP). Here, the length scales, from which the main contributions of the antiferromagnetic fluctuations stem, are relatively long range. Physically, we can understand the damping simply from the fact that the quasiparticles live in a bath of bosonic spin fluctuations. The quasiparticle can scatter at these fluctuations, resulting in a reduced life time, i.e., a larger imaginary part of the self energy.

Entering the crossover regime from the metallic side, the local correlations are strongly enhanced and entail strong non-local correlations in the vicinity of the antiferromagnetic phase transition. This can be seen for $U = 1.5D$ in Fig. 9, where we find a strongly damped quasiparticle peak and a splitting of the Hubbard bands, which can be considered to be a precursor of the spin polaron side peaks which develop in the antiferromagnetic phase.⁷⁹⁾

Finally, in the more insulating-like part of the crossover regime, at $U = 2D$ the antiferromagnetic correlations become even stronger, albeit they are now more

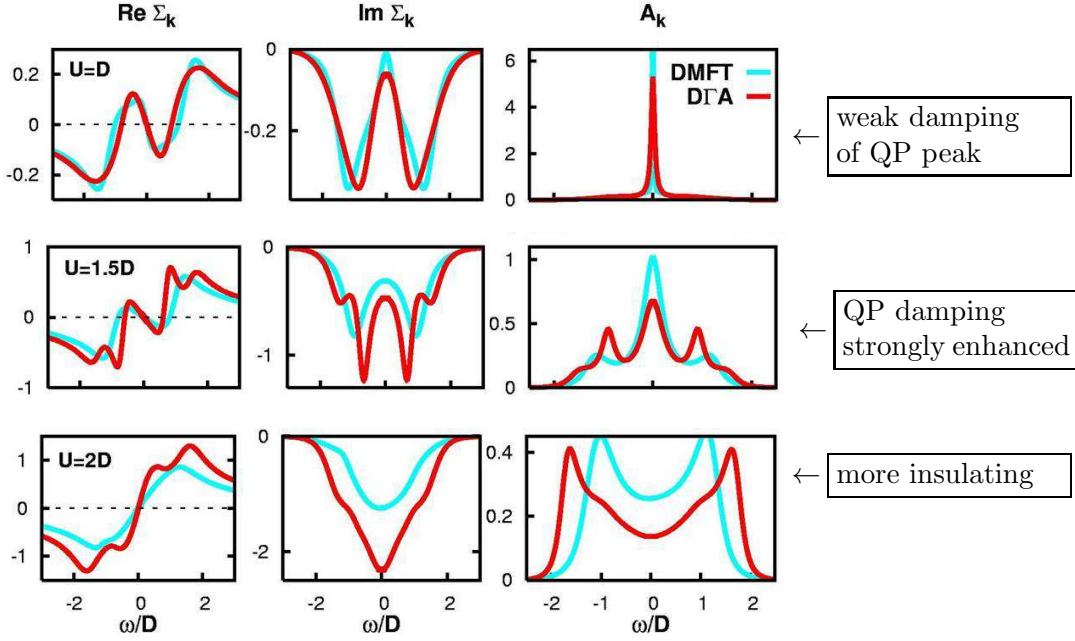


Fig. 9. DΓA self energy (left: real part, middle: imaginary part) and spectral function (right) at a point $\mathbf{k} = (\pi/2, \pi/2, \pi/2)$ on the Fermi surface for $U = 1D$ (top), $1.5D$ (central), and $2D$ (bottom) [blue/light grey line]. In the boxes on the right hand side we note the most important differences in comparison with DMFT [red/dark grey line]. [reproduced from Ref. 44)]

short range in nature. The paramagnetic phase becomes hence considerably more insulating, indicating a shift of the Mott-Hubbard transition towards lower values of U . It also shows that the Mott-Hubbard transition is strongly affected by antiferromagnetic fluctuations.

The results shown here are close to the antiferromagnetic phase transition, where the antiferromagnetic fluctuations are particularly strong. If we increase temperature, i.e., if we are deep inside the paramagnetic phase, the difference between DΓA and DMFT becomes very small. Already for $T > 2T_N$, i.e., twice the Néel temperature, the differences are minor.

All results shown were obtained without λ correction; and in three dimensions the λ correction has only a minor (quantitative) effect. It reduces the antiferromagnetic transition temperature T_N since T_N is somewhat overestimated in DMFT. But the same quantitative effects as in Fig. 9 occur also with λ correction albeit at this lower T_N , see Ref. 46).

3.2. Two-dimensional Hubbard model

Let us turn now to the two-dimensional Hubbard model on a square lattice where antiferromagnetic fluctuations are expected to be much more pronounced since the particle-hole ladder diagrams diverges logarithmically in two dimensions. Our insight into these antiferromagnetic fluctuations has been recently improved not only by the cluster extensions of DMFT dealing with short-range correlations, but also by the

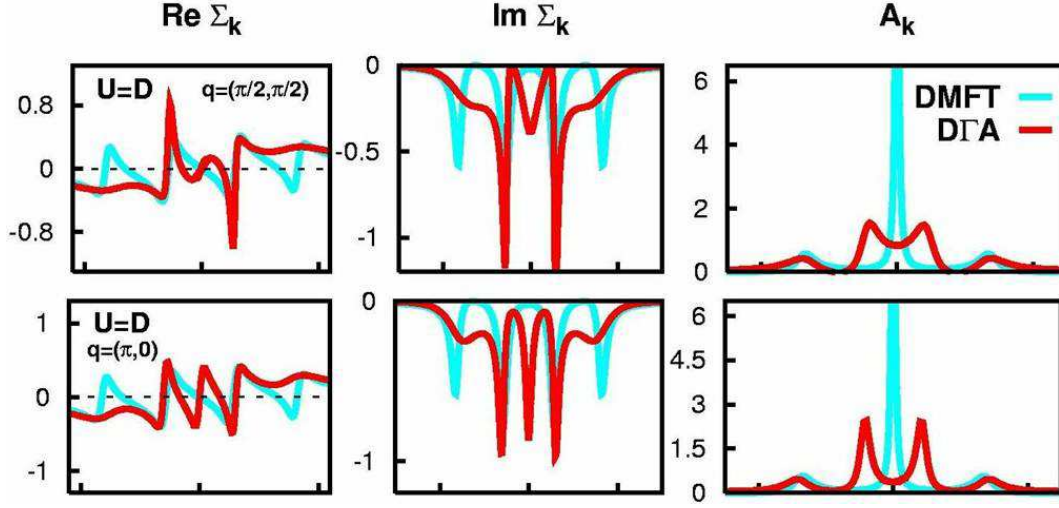


Fig. 10. Same as in Fig. 9 but for the two-dimensional Hubbard model and a single value of $U = D$ at $\beta = 17$. Shown are results for two different \mathbf{k} points on the Fermi surface, in the nodal (upper panel) and anti-nodal direction (lower panel). The antiferromagnetic fluctuations lead to a complete redistribution of the spectrum in the region of the quasiparticle peak; a pseudogap opens.

functional renormalization group method.^{80)–82)} The latter is very complementary to the cluster extensions since fRG deals with correlations on all length-scales, but as a (renormalized) perturbative approach it does not include the effects of strong correlations such as the Mott-Hubbard transition and strong renormalizations of the quasiparticle bands. In D Γ A, we cover both of these aspects, strong correlations and multiple length scales, in a single approach.

Let us emphasize that in two-dimensions the Moriya-esque λ correction of Section 2.3 is certainly important to obtain accurate results since otherwise the antiferromagnetic transition temperature T_N would be, without λ correction, much too high, i.e., at its DMFT mean field value – instead of zero as required by the Mermin-Wagner theorem. Nonetheless, we will present here results without this λ correction which can be compared with the reliable λ -corrected results of Ref. 46).

Figure 10 shows the same real and imaginary part of the self energy and spectral function as in the first line of Figure 9 for $U = D$, but now for two-dimensions (where the effective bandwidth is $D \equiv 4t$). The difference to three dimensions is dramatic since in two-dimensions the antiferromagnetic fluctuations lead to a complete redistribution of the spectrum. The quasiparticle peak of DMFT is swallowed up in a pseudogap. Even at a relatively weak interaction strength $U = D$, the effects of antiferromagnetic fluctuations are much more pronounced than for a much stronger interaction strength in three dimensions. Also the \mathbf{k} -dependence is dramatic, in contrast to three dimensions, where we only showed results for one \mathbf{k} -point because of the weak \mathbf{k} -dependence. Instead, in two dimensions, the comparison

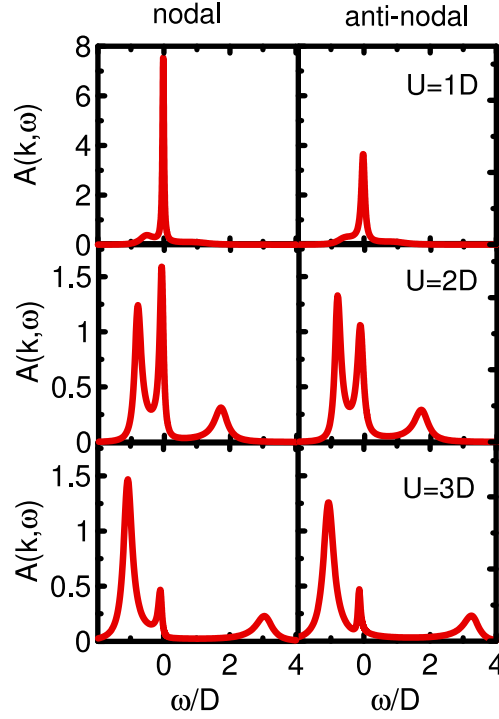


Fig. 11. Spectral function for the two-dimensional Hubbard model off half-filling in the nodal (left) and anti-nodal (right) direction. Parameters are $n \approx 0.8$ electrons/site, a next-nearest neighbor hopping $t' = 0.3t$, $\beta = 100$ and different values of the interaction $U = 1D$, $2D$, and $3D$ as indicated.

of nodal [$\mathbf{k} = (\pi/2, \pi/2)$] and anti-nodal direction [$\mathbf{k} = (\pi, 0)$] shows a strongly anisotropic pseudogap. If we would increase temperatures away from the antiferromagnetic phase transition, the pseudogap would hence first turn metallic in the nodal direction.

Fig. 11 presents results off half-filling for the asymmetric Hubbard model with $t' = 0.3t$ in a notation where t and t' have opposite prefactors. At weak coupling, $U = 1D$, we clearly see a quasiparticle peak which is already somewhat damped by antiferromagnetic fluctuations; Hubbard side bands are hardly visible. Note, however the strong anisotropy of the damping which is much stronger in the anti-nodal direction. Increasing U to $2D$, the damping becomes stronger, but also more isotropic. Spectral weight is transferred to the Hubbard side bands. Upon further increasing U to $3D$, these tendencies continue. The quasiparticle weight is very small; and the corresponding quasiparticle peak is strongly damped in an almost identical way for the nodal and anti-nodal direction. As we noted already for the three-dimensional Hubbard model, the antiferromagnetic fluctuations for weak coupling are very long-ranged explaining the pronounced difference between nodal and anti-nodal direction. The strong non-local correlations at larger U are somewhat more short-range in nature. Consequently, the anisotropy is not so pronounced.

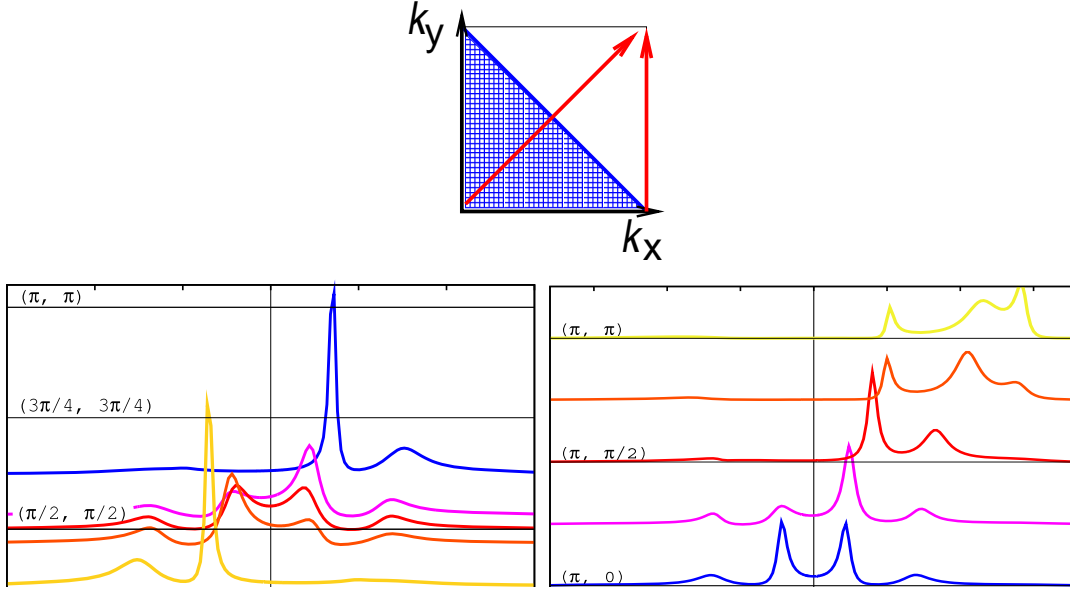


Fig. 12. Spectral function of the two-dimensional Hubbard model for different \mathbf{k} -points along the two high symmetry lines indicated in the upper panel, i.e., in the nodal and anti-nodal direction respectively.

For comparison with angular resolved photoemission experiments, we also provide a scan through the Brillouin zone along lines of high symmetry (in the nodal and anti-nodal direction), see upper panel of Fig. 12. Note, that $t' = 0$ so that the line $(0,0) \rightarrow (\pi,0)$ is connected to the (shown) line $(\pi,0) \rightarrow (\pi,\pi)$ by particle-hole symmetry. When approaching the Fermi surface, the (low-energy) quasiparticle peak moves towards the Fermi energy. However, this movement stops at some point inducing a pseudogap. Let us note that with the λ -correction the antiferromagnetic fluctuations are weaker than without λ correction⁴⁶⁾ but nonetheless still very strong. As a consequence, the pseudogap survives only in the anti-nodal direction.

Most recently, Li *et al.*⁸³⁾ calculated also the D Γ A lattice susceptibility. The results were obtained without λ -correction and are similar to those from the dual Fermion approach at higher temperatures (and much better than DMFT). However, at lower temperatures there are deviations since without λ correction D Γ A overestimates antiferromagnetic fluctuations.

3.3. One-dimensional Hubbard model

One of the fascinating effects of electronic correlation is the separation of spin and charge in one dimension. Slezak *et al.*⁴⁶⁾ addressed this issue in their one-dimensional D Γ Aesque calculation. As a starting point the authors considered an 8-site DCA cluster and supplemented it with additional longer range correlation as in the D Γ A, albeit with a restriction of the vertex to the second order diagrams shown in Fig. 13.

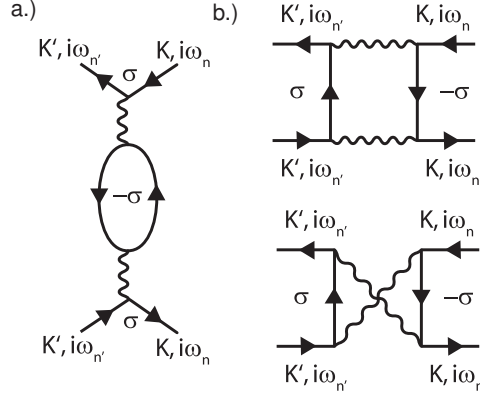


Fig. 13. Second order diagrams of the $D\Gamma$ Aesque calculation by Slezak *et al.* for the one-dimensional Hubbard model. [reproduced from Ref. 46)].

This way, the authors were able to go to a much larger number of lattice sites N_c than in DCA, see Fig. 14. This allowed Slezak *et al.* to conclude that for $N_c \rightarrow \infty$, spin and charge velocity are different so that an electron-like spin-charge excitation separates into its spin and charge components with time. This indicates that the inclusion of non-local correlations results in a non-Fermi-liquid phase, suggestively a Luttinger liquid.

§4. Summary and Outlook

In summary, we have presented the $D\Gamma$ A approach in an algorithmic form, including the restriction to the two particle-hole channels and the Moriyasque λ -correction. Let us also emphasize here that $D\Gamma$ A is a complementary approach to the extended DMFT (EDMFT)^{84),85)} EDMFT deals with the *local* correlations induced by non-local interactions, whereas $D\Gamma$ A deals with the *non-local* correlations stemming from a local interaction. The results for the Hubbard model in $d = 3, 2$, and 1 dimension show effects of antiferromagnetic fluctuations such as the damping of the quasiparticle peak and the shift of the Mott-Hubbard transition to lower values of U in three dimensions, the opening of a pseudo-gap and strong anisotropy of the spectrum in two-dimensions, and the spin-charge separation in one dimension.

Since short- and long-range range antiferromagnetic fluctuations are treated on the same footing with a numerical effort much more manageable than for cluster extensions of DMFT, we see excellent prospects for this approach in the future.

On a model level, a variety of fascinating phenomena can be addressed such as magnons, quantum criticality and the interplay of antiferromagnetic fluctuations and superconductivity. But also realistic multi-orbital calculations are possible for which the cluster extensions are too severely restricted because of the numerical effort. Such local density approximation (LDA) + $D\Gamma$ A calculations would, among others, allow

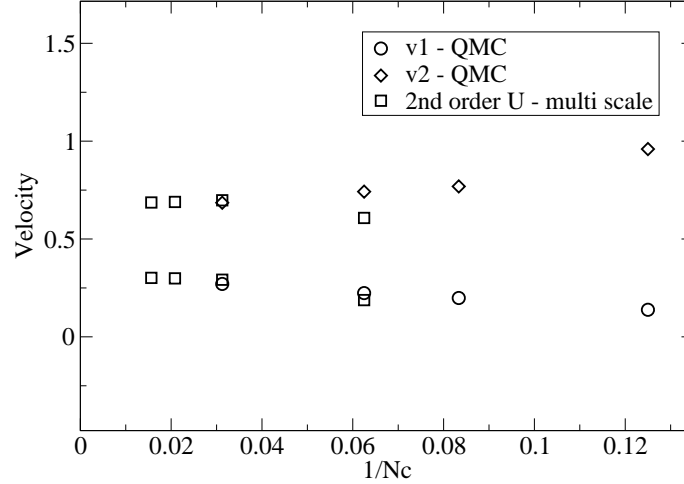


Fig. 14. Spin and charge velocity as a function of system size N_c calculated by DCA (triangles, circles) and D Γ A with a 8-site cluster as a starting point (squares). The parameters for the one-dimensional Hubbard model where $U = W = 1$ (W : bandwidth), $k = \pi/2$, $n = 0.7$ electrons/site, and inverse temperature $\beta = 31$. [reproduced from Ref. 46)].

us to study the effect of antiferromagnetic fluctuations on the Mott-Hubbard transition in V_2O_3 where the model scenario of Section 3.1 is realized in an actual material and which was previously studied successfully in LDA+DMFT.^{86)–90)} We hope that this review, along the lines of a talk given at the Yukawa Institute in November 2007, will stimulate more groups to apply the D Γ A approach to challenging problems of strongly correlated electron systems.

Acknowledgements

We thank the Yukawa Institute in Kyoto, Japan, for its generous hospitality and W. Metzner, M. Capone, C. Castellani, G. Sangiovanni, and R. Arita for stimulating discussions; we are indebted to M. Capone also for providing the DMFT(ED) code which has served as a starting point. This work was supported by the Russian Basic Research Foundation through Grant No. 747.2003.2 (AK).

References

- 1) W. Metzner and D. Vollhardt, Phys. Rev. Lett. **62** (1989), 324.
- 2) A. Georges and G. Kotliar, Phys. Rev. B **45** (1992), 6479.
- 3) A. Georges, G. Kotliar, W. Krauth, and M. Rozenberg, Rev. Mod. Phys. **68** 13 (1996).
- 4) G. Kotliar and D. Vollhardt, Physics Today **March** 53 (2004).
- 5) R. Bulla, Phys. Rev. Lett. **83** (1999), 136.
- 6) M. Jarrell, Phys. Rev. Lett. **69** (1992), 168.
- 7) K. Held, M. Ulmke, N. Blümer and D. Vollhardt, Phys. Rev. B **56** (1997), 14469.
- 8) M. Ulmke, Eur. Phys. J. B **1**, (1998) 301;

- 9) N. Furukawa, J. Phys. Soc. Jap. **63** (1994), 3214.
- 10) K. Held and D. Vollhardt, Euro. Phys. J. B **5** (1998).
- 11) I. A. Nekrasov, K. Held, G. Keller, D. E. Kondakov, T. Pruschke, M. Kollar, O. K. Andersen, V. I. Anisimov and D. Vollhardt, Phys. Rev. B **73**, 155112 (2006).
- 12) K. Byczuk, M. Kollar, K. Held, Y.-F. Yang, I. A. Nekrasov, T. Pruschke and D. Vollhardt, Nature Physics **3** 168 (2007).
- 13) A. Toschi, M. Capone, C. Castellani, and K. Held, arXiv:0712.3723.
- 14) V. I. Anisimov, A. I. Poteryaev, M. A. Korotin, A. O. Anokhin and G. Kotliar, J. Phys. Cond. Matter **9** (1997), 7359.
- 15) A. I. Lichtenstein and M. I. Katsnelson, Phys. Rev. B **57** 198, 6884 (1998).
- 16) K. Held, I. A. Nekrasov, G. Keller, V. Eyert, N. Blümer, A. McMahan, R. Scalettar, T. Pruschke, V. I. Anisimov and D. Vollhardt, phys. stat. sol. (B) **243** 2599 (2006).
- 17) G. Kotliar, S. Y. Savrasov, K. Haule, V. S. Oudovenko, O. Parcollet and C. A. Marianetti, Rev. Mod. Phys. **78**, 865 (2006).
- 18) K. Held, Adv. Phys. **56**, 829 (2007).
- 19) T. A. Maier, M. Jarrell, T. Pruschke, M. H. Hettler, Rev. Mod. Phys. **77**, 1027 (2005).
- 20) G. Kotliar, S. Y. Savrasov, G. Pálsson, and G. Biroli, Phys. Rev. Lett. **87**, 186401 (2001).
- 21) A. I. Lichtenstein and M. I. Katsnelson, Phys. Rev. B **62**, R9283 (2000).
- 22) M. Capone and G. Kotliar Phys. Rev. B **74**, 054513 (2006).
- 23) M. H. Hettler, A. N. Tahvildar-Zadeh, M. Jarrell, T. Pruschke, and H. R. Krishnamurthy, Phys. Rev. B **58**, (1998) 7475.
- 24) C. Huscroft, M. Jarrell, Th. Maier, S. Moukouri, and A. N. Tahvildarzadeh, Phys. Rev. Lett. **86**, 139 (2001).
- 25) Cluster sizes can be extended by using the fluctuation exchange approximation²⁶⁾ see K. Aryanpour, M. H. Hettler, and M. Jarrell, Phys. Rev. B **67**, 085101 (2003).
- 26) N. E. Bickers, D. J. Scalapino, and S. R. White, Phys. Rev. Lett. **62**, 961 (1989).
- 27) M. Potthoff, Eur. Phys. J. B **32** 429 (2003).
- 28) M. Potthoff and M. Balzer Phys. Rev. B **75**, 125112 (2007).
- 29) A. Schiller and K. Ingersent, Phys. Rev. Lett. **75** 113 (1995).
- 30) G. Zaránd, D. L. Cox and A. Schiller, Phys. Rev. B **62** 16227 (R) (2000).
- 31) M. Capone, M. Civelli, S. S. Kancharla, C. Castellani and G. Kotliar, Phys. Rev. B **69** 195105 (2004).
- 32) E. Koch, G. Sangiovanni, and O. Gunnarsson, arXiv:0710.1247.
- 33) T. Maier, M. Jarrell, T. Pruschke and J. Keller, Phys. Rev. Lett. **85** 1524 (2000).
- 34) T. A. Maier, M. Jarrell, T. C. Schulthess, P. R. C. Kent and J. B. White, Phys. Rev. Lett. **95** 237001 (2005).
- 35) R. Arita and K. Held, Phys. Rev. B **73** 064515 (2006).
- 36) A. I. Poteryaev, A. I. Lichtenstein and G. Kotliar, Phys. Rev. Lett. **93** 086401 (2004).
- 37) V. V. Mazurenko, A. I. Lichtenstein, M. I. Katsnelson, I. Dasgupta, T. Saha-Dasgupta and V. I. Anisimov, Phys. Rev. B **66** 081104 (R) (2002).
- 38) S. Biermann, A. Poteryaev, A. I. Lichtenstein and A. Georges, Phys. Rev. Lett. **94** 026404 (2005).
- 39) R. Blankenbecler, D. J. Scalapino and R. L. Sugar, Phys. Rev. D **24** 2278 (1981).
- 40) E. Z. Kuchinskii *et al.*, Sov. Phys. JETP Lett. **82**, 98 (2005).
- 41) M. V. Sadovskii *et al.*, Phys. Rev. B **72**, 155105 (2005).
- 42) A. N. Rubtsov, M. I. Katsnelson, and A. I. Lichtenstein, Phys. Rev. B **77**, 033101 (2008); S. Brener, H. Hafemann, A. N. Rubtsov, M. I. Katsnelson, and A. I. Lichtenstein, Phys. Rev. B **77**, 195105 (2008).
- 43) V. I. Tokar and R. Monnier, cond-mat/0702011 (unpublished).
- 44) A. Toschi, A. A. Katanin, and K. Held, Phys. Rev. B **75**, 045118 (2007).
- 45) A. A. Katanin, A. Toschi, and K. Held, (unpublished).
- 46) C. Slezak, M. Jarrell, Th. Maier, and J. Deisz, cond-mat/0603421 (unpublished).
- 47) H. Kusunose, J. Phys. Soc. JPN. **75**, 054713 (2006).
- 48) J. E. Hirsch and R. M. Fye, Phys. Rev. Lett. **56** 2521 (1986).
- 49) M. Feldbacher, K. Held and F. F. Assaad, Phys. Rev. Lett. **96** 139702 (2006).
- 50) A. N. Rubtsov and A. I. Lichtenstein, JETP Lett. **80** 61 (2004).
- 51) P. Werner and A. J. Millis, Phys. Rev. B **74** 155107 (2006).
- 52) S. Sakai, R. Arita, K. Held and K. Aoki, Phys. Rev. B **74** 155102 (2006).

- 53) Y. A. Bychkov, L. P. Gorkov, and I. E. Dzyaloshinskii, Zh. Exp. Teor. Fiz. **50**, 738 (1966) [Sov. Phys. JETP **23**, 489 (1966)].
- 54) N. E. Bickers and S. R. White, Phys. Rev. B **43**, 8044 (1991).
- 55) V. Janiš, Phys. Rev. B **60** 11345 (1999).
- 56) T. Moriya, “Spin fluctuations in Itinerant Electron Magnetism” (Springer, 1985).
- 57) N. F. Mott, Rev. Mod. Phys. **40**, 677 (1968); *Metal-Insulator Transitions* (Taylor & Francis, London, 1990)
- 58) F. Gebhard, *The Mott Metal-Insulator Transition* (Springer, Berlin, 1997).
- 59) A. Liebsch, Europhys. Lett. **63** 97 (2003).
- 60) A. Liebsch, Phys. Rev. Lett. **91** 226401 (2003).
- 61) A. Koga, N. Kawakami, T. M. Rice and M. Sgrist, Phys. Rev. Lett. **92** 216402 (2004).
- 62) A. Liebsch, Phys. Rev. B **70** 165103 (2005).
- 63) A. Koga, K. Inaba and N. Kawakami, Prog. Theo. Phys. Suppl. **160** 253 (2005).
- 64) A. Koga, N. Kawakami, T. M. Rice and M. Sgrist, Phys. Rev. B **72** 045128 (2005).
- 65) K. Inaba, A. Koga, S. I. Suga and N. Kawakami, J. Phys. Soc. Jap. **74** 2393 (2005).
- 66) K. Inaba, A. Koga, S. I. Suga and N. Kawakami, Phys. Rev. B **72** 085112 (2005).
- 67) S. Biermann, L. de’ Medici and A. Georges, Phys. Rev. Lett. **95** 206401 (2005).
- 68) L. de’ Medici, A. Georges and S. Biermann, Phys. Rev. B **72** 205124 (2005).
- 69) R. Arita and K. Held, Phys. Rev. B **72** 201102(R) (2005).
- 70) C. Knecht, N. Blümer and P. G. J. van Dongen, Phys. Rev. B **72** 081103 (R) (2005).
- 71) A. Liebsch, Phys. Rev. Lett. **95** 116402 (2005).
- 72) P. G. J. van Dongen, C. Knecht and N. Blümer, Phys. Stat. Sol. B **243** 116 (2006).
- 73) M. Ferrero, F. Becca, M. Fabrizio and M. Capone, Phys. Rev. B **72** 205126 (2005).
- 74) A. Liebsch and T. A. Costi, Euro. Phys. J. B **51**, 523 (2006).
- 75) N. Blümer, C. Knecht, K. Pozgajic and P. van Dongen (2006), cond-mat/0609758.
- 76) A. Liebsch (2006), cond-mat/0610482.
- 77) S.-K. Mo, H.-D. Kim, J. W. Allen, G.-H. Gweon, J. D. Denlinger, J.-H. Park, A. Sekiyama, A. Yamasaki, S. Suga, P. Metcalf, and K. Held, Phys. Rev. Lett. **93** 076404 (2004).
- 78) L. Baldassarre, A. Perucchi, D. Nicoletti, A. Toschi, G. Sangiovanni, K. Held, M. Capone, M. Ortolani, L. Malavasi, M. Marsi, P. Metcalf, P. Postorino, and S. Lupi, Phys. Rev. B **77**, 113107 (2008)
- 79) G. Sangiovanni, A. Toschi, E. Koch, K. Held, M. Capone, C. Castellani, O. Gunnarsson, S.-K. Mo, J. W. Allen, H.-D. Kim, A. Sekiyama, A. Yamasaki, S. Suga and P. Metcalf, Phys. Rev. B **73** 205121 (2006).
- 80) D. Zanchi and H. J. Schulz, Phys. Rev. B **54**, 9509 (1996).
- 81) C. J. Halboth and W. Metzner, Phys. Rev. Lett. **85**, 5162 (2000); C. Honerkamp *et al.*, Phys. Rev. B **63**, 035109 (2001); Phys. Rev. Lett. **87**, 187004 (2001).
- 82) A. A. Katanin and A. P. Kampf, Phys. Rev. B **68**, 195101 (2003).
- 83) G. Li, H. Lee, and H. Monien, arXiv:0804.3043.
- 84) Q. Si and J.L. Smith, Phys. Rev. Lett. **77**, 3391 (1996).
- 85) H. Kajueter, Ph.D. thesis, Rutgers University (1996).
- 86) K. Held, G. Keller, V. Eyert, V. I. Anisimov and D. Vollhardt, Phys. Rev. Lett. **86** 5345 (2001).
- 87) G. Keller, K. Held, V. Eyert, D. Vollhardt and V. I. Anisimov, Phys. Rev. B **70** 205116 (2004).
- 88) M. S. Laad, L. Craco and E. Müller-Hartmann, Phys. Rev. Lett. **91** 156402 (2003).
- 89) M. S. Laad, L. Craco and E. Müller-Hartmann, Phys. Rev. B **73** 045109 (2006).
- 90) A.I. Poteryaev, J.M. Tomczak, S. Biermann, A. Georges, A.I. Lichtenstein, A.N. Rubtsov, T. Saha-Dasgupta and O.K. Andersen, Phys. Rev. B **76**, 085127 (2007).